Directive properties of active coated nano-particles

Arslanagic, Samel; Ziolkowski, Richard W.

Publication date:
2012

Directive properties of active coated nano-particles

Samel Arslanagić[1*], and Richard W. Ziolkowski[2]

[1]Department of Electrical Engineering, Electromagnetic Systems,
Technical University of Denmark, Denmark
[2]Department of Electrical and Computer Engineering, University of Arizona, USA
*corresponding author, E-mail: sar@elektro.dtu.dk

Abstract

The directivities of the fields radiated by a variety of cylindrical and spherical active coated nano-particles, which are excited by their respective sources of illumination at optical frequencies, are investigated. Particular attention is devoted to the influence of the source location and optical gain constant on the directivities. While significant variations in the directivities are realized in the cylindrical cases for different source locations within and slightly outside the nano-particles and values of the optical gain constant, the corresponding spherical cases exhibit negligible differences.

1. Introduction

The performance of electrically small antennas (ESAs) is constrained by certain conventional limitations. For instance, if not matched properly, they are very inefficient radiators of electromagnetic energy, due to their intrinsic non-resonant nature, with accompanying low directivities [1]. While a variety of traditional matching techniques exist, the recent advent in metamaterial (MTM) research has, among other things, fostered truly novel means of matching ESAs [2]. In particular, the use of double-negative (DNG), epsilon-negative (ENG), and/or mu-negative (MNG) MTMs was found to lead to interesting and highly resonant properties in sub-wavelength configurations when properly combined with ordinary double-positive (DPS) materials [2]-[5]. These resonances were exploited in [6] and [7], where efficient MTM-based ESAs were proposed, and in [8] where MTM-inspired electrically small near-field parasitic resonators were used as impedance transformers to realize matching of the overall antenna system to its source and to the wave impedance of the medium in which it radiates. While the above works focused on radio and microwave frequencies, similar highly resonant properties, for potential use in nano-sensing, -amplifying and -antenna applications, were reported for passive plasmonic-based configurations at optical frequencies, see e.g., [9], [10] and the works referenced therein, as well as *active* plasmonic-based configurations, see e.g., [11] and the works referenced therein, as well as [12] and [13]. In particular, interesting enhancements of directivity patterns for higher order mode sub-wavelength radiators made of DPS materials in conjunction with passive MTMs or plasmonic materials, were reported in [10], this providing an alternate route towards sub-wavelength radiators with high directivities.

The present work examines the directivity properties of nano-antennas consisting of active coated nano-particles (CNPs) of cylindrical and spherical shape excited by their respective sources of illumination at optical frequencies. For spherical CNPs, the source of excitation is an electric Hertzian dipole, which is taken to be normal as well as tangential to surfaces of the CNP, while for cylindrical CNPs, the source of excitation is an infinitely long magnetic line source (MLS). The CNPs emphasized inhere are all made of a silica nano-core and are layered with a concentric silver nano-shell; however, other variations in the materials of the CNP can be easily accounted for. The gain is introduced inside the dielectric part of the CNP, i.e., the nano-core, via the so-called canonical, constant frequency, gain model. This work constitutes an extension of [12] and [13] where detailed near-field studies have revealed super-resonant properties of the examined active CNPs despite their very small electrical sizes. Particular attention is devoted to the influence of the source location and the optical gain constant on the resulting directivity patterns. In the cylindrical case, it is shown how the directivity of a super-resonant CNP can be re-shaped by either changing the location of the MLS or adjusting the value of the optical gain constant. As to the spherical CNPs, the resulting directivity patterns are shown to be unaffected by the presence of the CNP - even in its super-resonant state for which large amounts of the radiated power are extracted from the source – and they largely correspond to the pattern of an isolated dipole. Thus, as in the passive spherical case [10], the dipolar resonance excited inside the examined active spherical CNPs does not modify the directivity pattern of the exciting Hertzian dipole, but rather enhances its total radiated power.

This paper is organized as follows. Section 2 presents the configurations to be discussed, while the methods of their analysis and the associated analytical results are summarized in Section 3. The numerical results are presented in Section 4, and the entire work is summarized and concluded in Section 5. Throughout the work, the time factor $\exp(j\omega t)$, with ω being the angular frequency, and t being the time, is assumed and suppressed.

2. Configurations

We consider both cylindrical (Figure 1a)) and spherical (Figure 1b)) CNPs.

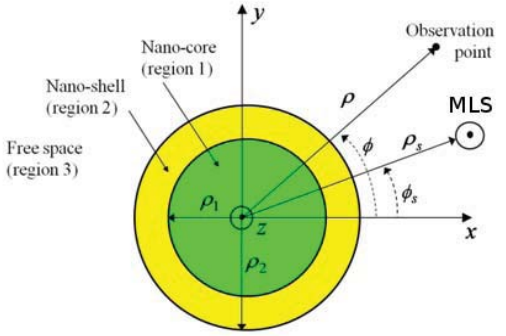

(a)

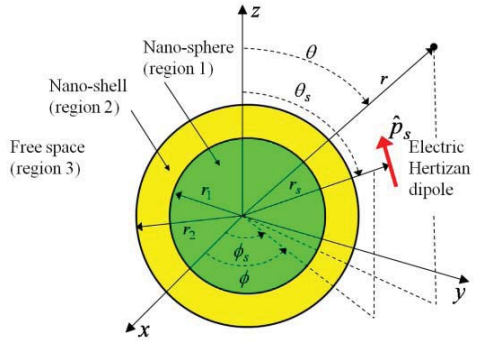

(b)

Figure 1: The cylindrical (a), and spherical (b) CNP configurations.

In both cases, they are comprised of a dielectric nano-core covered concentrically with a plasmonic nano-shell, and are immersed in free-space, which has the permittivity, ε_0, permeability, μ_0, and thus the intrinsic impedance $\eta_0 = \sqrt{\mu_0 / \varepsilon_0}$ and wave number $k_0 = \omega\sqrt{\varepsilon_0\mu_0} = 2\pi / \lambda$, where λ denotes the free-space wavelength.

For the cylindrical CNP, the inner and outer radii of the nano-shell are denoted by ρ_1 and ρ_2, respectively. The CNP is illuminated by the field generated by an arbitrarily located infinitely long magnetic line source (MLS) possessing a constant magnetic current I_m [V/m]. A circular cylindrical coordinate system, with the coordinates (ρ, ϕ, z) and an associated rectangular coordinate system (x, y, z) are introduced such that their origins coincide with the cross-sectional center of the CNP. Furthermore, the entire CNP-MLS configuration is infinite in the *z*-direction, with the MLS being parallel to the axis of the cylinders. The coordinates of the observation point are (ρ, ϕ), and those of the MLS are (ρ_s, ϕ_s).

For the spherical CNP, the inner and outer radii of the nano-shell are denoted by r_1 and r_2, respectively. The CNP is illuminated by the field generated by an arbitrarily oriented and located electric Hertzian dipole (EHD) with the dipole moment $\vec{p} = \hat{p}_s p_s$, where $\hat{p}_s$ is its orientation and p_s [Am] is its complex amplitude. A spherical coordinate system (r, θ, ϕ) and the associated rectangular coordinate system (x, y, z) are introduced such that the origin of these coincide with the center of the CNP. The coordinates of the observation point are (r, θ, ϕ), and those of the EHD are (r_s, θ_s, ϕ_s).

3. Analytical results

The analytical solutions for the problems shown in Figure 1 have been derived in [4] and [5], and are used here to study the directivity of these configurations.

For the cylindrical CNP configurations, the solution procedure is as follows. The field due to the MLS, which constitutes the known incident field, is expanded in terms of cylindrical wave functions. This is likewise the case with the unknown scattered fields due to the CNP in the three regions. The fields due to the CNP involve the unknown expansion coefficients $C_{i,n}$, where $i = 1$ for the field in region 1, $i = 2$ and 3 for the field in region 2, and $i = 4$ for the field in region 3, and where the symbol n is the mode number ($n = 0$ is the monopole mode in the expansion, $n = 1$ is the dipole mode, etc. for the other modes). The unknown expansion coefficients depend on the location of the MLS and are obtained by enforcing the boundary conditions at the two cylindrical interfaces, $\rho = \rho_1$ and $\rho = \rho_2$. With the exact field solutions at hand, the directivity, *D*, defined as the ratio of the radiation intensity to the total average power per unit angle, can be expressed as [4]

$$D(\phi) = \frac{2 \cdot \left| \sum_{n=0}^{N_{\max}} \tau_n j^n \alpha_n \cos[n(\phi - \phi_s)] \right|^2}{\sum_{n=0}^{N_{\max}} \tau_n^2 (3 - \tau_n) |\alpha_n|^2}, \qquad (1)$$

where $\alpha_n = C_{4,n}$ for the MLS inside the CNP, and $\alpha_n = J_n(k_0\rho_s) + C_{4,n}$ for the MLS outside the CNP. In these results, the function $J_n(\cdot)$ is the Bessel function of order n, τ_n is the Neumann number ($\tau_n = 1$ for the $n = 0$ mode and $\tau_n = 2$ otherwise), while $N_{\max}$ is the truncation limit in the implementation of the exact infinite summation chosen to ensure the convergence of the expansion in (1). The expression in (1) was used to study the directivity properties of sub-wavelength passive MTM-based particles in [4], and of super-resonant active CNPs in [13] for a variety of MLS locations.

For the spherical CNP configuration, the solution procedure is as follows. The field due to the EHD, which

constitutes the known incident field, is expanded in terms of transverse magnetic (TM) and transverse electric (TE) spherical waves with the known expansion coefficients $a_{nm}^{(c)}$ (TM coefficients), and $b_{nm}^{(c)}$, (TE coefficients), where the index c denotes the region in which the field is determined. The unknown scattered fields due to the CNP in the three regions are likewise expanded in terms of TM and TE spherical waves; these expansions involve the unknown TM and TE expansion coefficients denoted by $A_{i,nm}$ and $B_{i,nm}$, respectively, where $i = 1$ for the field in region 1, $i = 2$ and 3 for the field in region 2, and $i = 4$ for the field in region 3. These expansion coefficients depend on the EHD location and orientation, and are easily obtained by enforcing the boundary conditions on the two spherical interfaces, $r = r_1$ and $r = r_2$. The general field solutions have been obtained in [5] and are specialized here for the far-field observation points in order to derive an expression for the directivity of the configuration in Figure 2b). In particular, the directivity takes on the form,

$$D(\theta,\phi) = \frac{2\pi}{\eta_0}\frac{1}{P_t}\left(\left|F_{t,\theta}\right|^2 + \left|F_{t,\phi}\right|^2\right), \tag{2}$$

where

$$F_{t,\theta} = \sum_{n=1}^{N_{\max}}\sum_{m=-n}^{n} j^{n-1}e^{jm\phi} \times \left[\frac{1}{\omega\varepsilon_0}\alpha_{nm}\frac{d}{d\theta}P_n^{|m|}(\cos\theta) + \beta_{nm}\frac{1}{k_0}\frac{jm}{\sin\theta}P_n^{|m|}(\cos\theta)\right], \tag{3a}$$

and

$$F_{t,\phi} = \sum_{n=1}^{N_{\max}}\sum_{m=-n}^{n} j^{n-1}e^{jm\phi} \times \left[\frac{1}{\omega\varepsilon_0}\alpha_{nm}\frac{jm}{\sin\theta}P_n^{|m|}(\cos\theta) - \beta_{nm}\frac{1}{k_0}\frac{d}{d\theta}P_n^{|m|}(\cos\theta)\right], \tag{3b}$$

are, respectively, the θ- and ϕ- components of the total radiation vector, $\boldsymbol{F}_t(\theta,\phi)$, which is related to the total far-field term $\boldsymbol{E}_t(\theta,\phi)$ through the relation $\boldsymbol{E}_t(\theta,\varphi) \approx \boldsymbol{F}_t(\theta,\varphi)\exp(-jk_0r)/r$. Moreover, the quantity P_t is the total radiated power, and is expressed as [5]

$$P_t = \frac{\pi}{\omega k_0}\sum_{n=1}^{N_{\max}}\sum_{m=-n}^{n} 2\frac{n(n+1)}{2n+1}\frac{(n+|m|)!}{(n-|m|)!}\left[\frac{|\alpha_{nm}|^2}{\varepsilon_0} + \frac{|\beta_{nm}|^2}{\mu_0}\right]. \tag{4}$$

In the above expressions, $\alpha_{nm} = A_{4,nm}$ and $\beta_{nm} = B_{4,nm}$, when the EHD is inside the two regions of the CNP, while $\alpha_{nm} = a_{nm}^{(4)} + A_{4,nm}$ and $\beta_{nm} = b_{nm}^{(4)} + B_{4,nm}$, when the EHD is outside the CNP [5]. Moreover, $P_n^{|m|}(\cdot)$ is the associated Legendre function of the first kind of degree n and order $|m|$, while the symbol $N_{\max}$ is the truncation limit in the implementation of the exact infinite summation chosen to ensure the convergence of the expansion in (2). While the expression for the total radiated power in (4) was used in [5] and [12], [14] to conduct a thorough analysis of sub-wavelength resonances in passive and active spherical CNPs, respectively, the directivity properties of such active particles on the basis of (2) have not been reported previously.

4. Numerical results and discussion

4.1. Background – sub-wavelength resonances in CNPs

Previous results [11]-[14] have demonstrated that highly resonant sub-wavelength CNPs can be designed by including gain, e.g., inside their nano-cores. This configuration was found to lead to scattering cross-sections that are orders of magnitude larger than the values predicted by their geometrical sizes, see e.g., [11] and the works referenced therein, as well as to the enormous radiated powers for localized excitation sources [12]-[14]. Significant attention in those works has been devoted to a CNP consisting of a silica nano-core of radius 24 nm, coated with a 6nm thick silver nano-shell for which the size-dependency of the permittivity was taken into account. The silica nano-core permittivity consisted of two contributions: one from its refractive index $n = \sqrt{2.05}$ in the frequency region of interest and another accounting for the canonical, constant frequency, gain model through which its permittivity reads $\varepsilon_1 = (n^2 - \kappa^2 - 2jn\kappa)\varepsilon_0$, where the parameter κ (optical loss or gain constant) determines the nature of the nano-core: lossless (and passive) for $\kappa = 0$, lossy and passive for $\kappa > 0$ (optical loss constant) and active for $\kappa < 0$ (optical gain constant). For such CNPs, the so-called super-resonant states, with very large radiated powers, were identified for the cylindrical case for $\kappa = -0.175$ at the excitation wavelength of $\lambda = 577.70$ nm, and for the spherical case for $\kappa = -0.245$ at the excitation wavelength of $\lambda = 502.1$ nm. These super-resonances are illustrated in Figure 2 in terms of the normalized radiation resistance (NRR), i.e., the ratio of the total power radiated when the source and the CNP are present to the total power radiated by the source in the absence of the CNP, as a function of the source location, x_s. The sources are located along the positive x-axis for both the cylindrical and the spherical Ag-based CNPs. For the cylindrical CNP, the MLS possesses a current amplitude $I_m = 1$ [V/m], while both x- as well as z- oriented EHDs have a dipole moment $p_s = 5\cdot10^{-9}$ [Am]. In what follows, the directivity properties of these Ag-based CNPs of cylindrical and spherical shape are thoroughly examined.

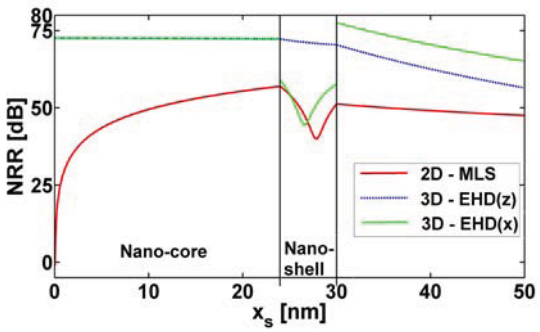

Figure 2: Normalized radiation resistance (NRR) as a function of the source location, x_s, along the positive x-axis for both the cylindrical (2D) and the spherical (3D) super-resonant Ag-based CNPs. In the latter case, the EHD is taken to be both x- and z-oriented. The nano-core and nano-shell regions are indicated in the figure.

4.2. Cylindrical CNPs

The large variations in the NRR shown in Figure 2, with the alternating MLS location in the cylindrical case were thoroughly explained in [13]. Here, it is of great interest to explore the directivity behavior of such configurations. As illustrated in Figure 3a), which shows the directivity (1) for the super-resonant ($\kappa = -0.175$; $\lambda = 577.70$ nm) Ag-based CNP for the indicated MLS locations along the positive x-axis within the nano-core, there are large variations in the resulting patterns. The directivity in the super-resonant state can be re-shaped from a perfectly monopolar pattern (attained at x_s = 0 nm) to a perfectly symmetric dipolar pattern (attained at x_s = 5nm) with small variations in the MLS location. The former case agrees well with the absence of any resonant phenomena observed in Figure 2 when the MLS is at or very near the center of the CNP (NRR around 0 dB). On the other hand, the latter case indicates a strong excitation (NRR around 45 dB for x_s = 5nm) of the dipolar mode necessary for the rapidly increasing NRR values in Figure 2 for MLS locations further away from the CNP center. These far-field results are in line with the near-field distributions reported for this Ag-based CNP configuration in [13]. The maximum directivity of 2 is found for the perfectly symmetric dipolar pattern in Figure 3a) along the $\phi = 0^\circ$ and $\phi = 180^\circ$ directions. However, larger values can be obtained for specific MLS locations (near the CNP center) for which the dominant mode is a mixture of a monopolar and dipolar modes, rather than the resonant dipolar mode alone. For instance, the result obtained for x_s = 0.1 nm given in Figure 3b) illustrates this point.

Apart from the pattern re-shaping possibilities with varying location of the MLS, it is interesting to note that adjustment of the optical gain constant κ for a given location of the source can likewise re-shape the overall directivity pattern. With reference to Figure 3b), which shows the directivity for the Ag-based CNP when the MLS is located at x_s = 5nm, the perfectly symmetric dipolar pattern attained in the super-resonant case can be re-shaped such that its main beam is along the $\phi = 0^\circ$ or $\phi = 180^\circ$ direction, depending on the value of κ. For the examined values of κ which are larger than the super-resonant value ($\kappa = -0.175$), the main beam (which is approaching a maximum directivity of 3) points in the $\phi = 180^\circ$ direction. In contrast, it points along the $\phi = 0^\circ$ direction for values of κ smaller than the super-resonant value.

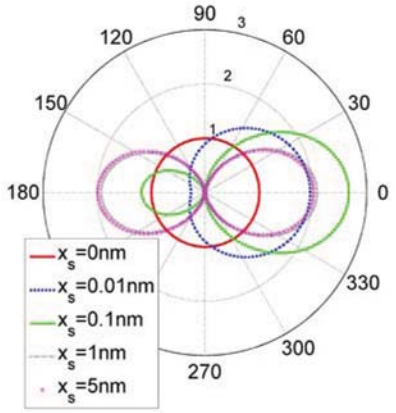

(a)

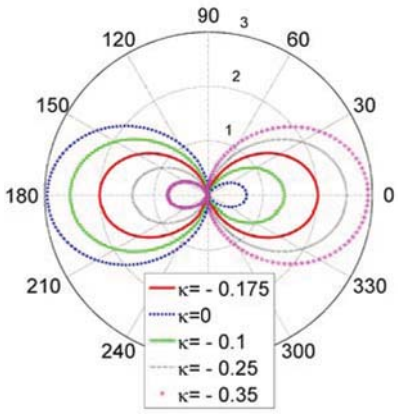

(b)

Figure 3: Directivity for the Ag-based CNP excited by a MLS. In (a), the CNP is super-resonant, and different MLS locations, x_s , inside the nano-core along the positive x-axis are considered. In (b), the MLS is located at x_s = 5nm and different values of the optical gain constant κ are considered.

Aside from these interesting results for the cylindrical Ag-based CNP, a few other remarks are in order. As explained in [13] using the near-field distribution results, the main reason for the peak amplitude changes of the NRR in Figure 2 is the difference in the coupling strength with the varying MLS location which determines the potency of the underlying resonant dipolar mode. As an example, the near-field of the resonant dipolar mode is significantly stronger for the MLS located near the nano-shell interface, e.g., at x_s = 23 nm, than inside the nano-shell at x_s = 28.74 nm, where the NRR experiences the dip shown in Figure 2. However,

once the MLS is sufficiently far away from the origin so that the perfectly symmetric dipolar pattern is obtained, as the one illustrated in Figure 3a) for x_s = 5 nm, the very same directivity pattern (of maximum directivity of 2) results also for other MLS locations inside the CNP, as well as outside of it at close distances. This is partly illustrated in Figure 4) which shows the directivity for three MLS locations inside the nano-shell of the super-resonant Ag-based CNP: near the first interface (x_s = 25 nm), at the location of minimum NRR inside the nano-shell (x_s = 27.84 nm), and near the second interface (x_s = 29 nm). In all cases, the same symmetric dipolar pattern is observed.

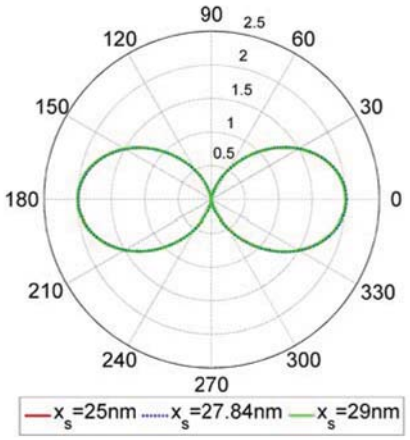

Figure 4: Directivity for the super-resonant Ag-based CNP excited by a MLS located at three different locations inside the nano-shell region of the particle.

Thus, once the MLS location is established away from the origin, the symmetric dipolar pattern is observed. Moreover, the explanation for the varying levels of the NRR found in Figure 2 cannot be revealed by inspecting the directivity patterns (*which are identical*), but rather the near-field distributions must be examined. Results essentially the same as those in Figure 4 are also obtained for MLS locations in the exterior of the CNP at sufficiently close distances to it.

It is furthermore interesting to parallel the above results with those of the corresponding sub-wavelength resonant MTM-based structures at radio frequencies [5]. In [5], an electric line source excitation of double-negative (DNG) or mu-negative (MNG) coated passive structures were examined. As remarked there, those results also apply, by duality, to epsilon-negative (ENG) coated passive structures excited by a MLS. The maximum NRR levels in [5] for the resonant cylindrical MTM-based structures are well below (with maximum NRR around 23 dB) those reported in Figure 2. Moreover, a complete symmetry in their dipolar directivity patterns was not obtained. In particular, for the source inside the ENG shell-region, asymmetric directivity patterns (which are each other's images with respect to *y*-axis) result for MLS locations near the first and the second shell interface. This is in sharp contrast to the results of Figure 4 where identical and completely symmetric patterns are obtained. In addition, since the NRR of the MTM-based structures in [5] drops to 0 dB for a particular source location inside the shell-region, the pattern re-shaping also occurs for altering source locations in this region. Specifically, for the minimum NRR location of the source inside the shell-region, a perfect monopolar pattern is obtained [5]. These findings for sub-wavelength resonant MTM-based ENG-coated passive structures, as those studied in [5], appear in sharp contrast to the above gain-enhanced results for the Ag-based active CNPs.

4.3. Spherical CNPs

Figure 2 reveals interesting differences between the *z*- and *x*-oriented EHD excitations of the super-resonant Ag-based spherical CNP, which were detailed through near-field investigations in [14].

Figure 5 shows the directivity of the Ag-based CNP for varying values of the parameter κ in the case of a *z*-oriented EHD excitation. The EHD has the dipole moment $p_s = 5 \cdot 10^{-9}$ [Am] and is located on the *x*-axis at +12 nm from the origin. Specifically, the E-plane (*xz*-plane) pattern results are shown in Figure 5a) and the H-plane (*xy*-plane) pattern results are shown in Figure 5b). Despite the large levels of the NRR, the directivity of the super-resonant state, which is clearly dipolar, is not enhanced relative to that of an isolated *z*-oriented EHD. In particular, its value remains around 1.5. Unlike the cylindrical case, there is a complete symmetry in the CNP and, consequently, no preferred axis. Moreover, the investigated values of κ are found, again because of the symmetry, to have only a negligible effect on the directivity. The directivity of the super-resonant Ag-based CNP is shown in Figure 5c) as a function of $\theta \in (0^o, 180^o)$ and $\phi \in (0^o, 360^o)$, clearly supporting the above observations.

For the *x*-oriented EHD excitation of the super-resonant Ag-based CNP, Figure 6 shows the resulting directivity. The E-plane (*xz*-plane) pattern is shown in Figure 6a); the H-plane (*yz*-plane) pattern is shown in Figure 6b). The directivity as a function of $\theta \in (0^o, 180^o)$ and $\phi \in (0^o, 360^o)$ is shown in Figure 6c). Except from the flipping of the E-plane pattern by 90° relative to the *z*-oriented EHD case in Figure 5a), the same over-all conclusions apply as with the *z*-oriented EHD case, i.e., the directivity is not enhanced by the presence of the super-resonant Ag-based CNP (for which large NRR values are obtained), its maximum value remains around 1.5 (which is that of an isolated EHD), and the H-plane (*xy*-plane) pattern is azimuthally symmetric. This behavior is again expected because of the spherical symmetry of the CNP. Thus, as in the passive spherical case [10], the dipolar resonance excited inside the examined active electrically small spherical CNPs does not modify the directivity pattern of the exciting Hertzian dipole, but rather reinforces it. Moreover, the varying NRR levels observed for the *x*-oriented EHD in Figure 2 cannot be revealed through the directivity pattern alone, but rather require studying the near-field distributions.

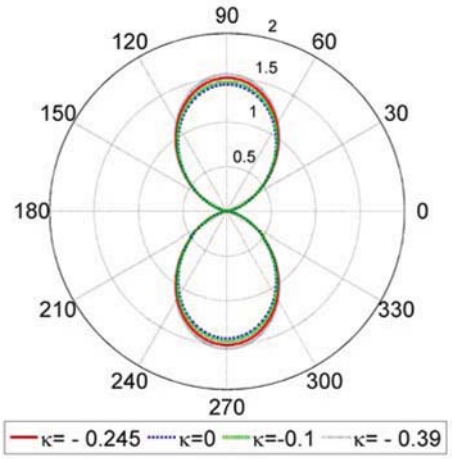

(a)

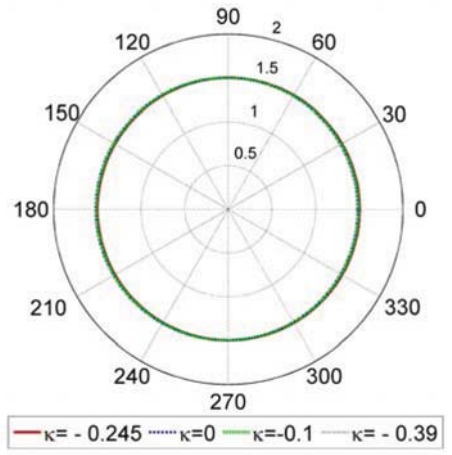

(b)

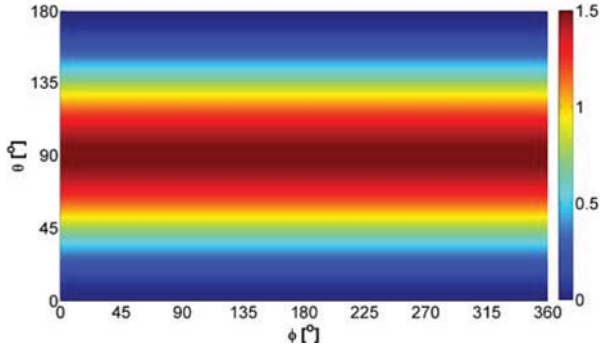

(c)

Figure 5: Directivity for the Ag-based CNP for a *z*-oriented EHD located along the *x*-axis at +12 nm for different values of the parameter κ. The E-plane (*xz*-plane) pattern results are shown in (a), and the H-plane pattern results (*xy*-plane) are shown in (b). In the case of the super-resonant Ag-based CNP, the directivity is shown in (c) for all values of θ and ϕ.

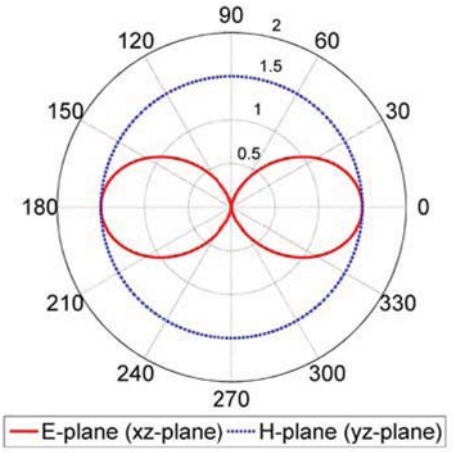

(a)

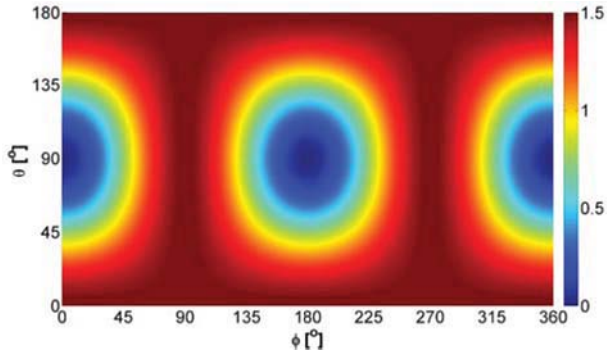

(b)

Figure 6: Directivity for the super-resonant Ag-based CNP for a *x*-oriented EHD located along the *x*-axis at 12 nm. The E-plane (*xz*-plane) results are shown in (a), the H-plane results (*yz*-plane) are shown in (b), while the results for all values of θ and ϕ are shown in (c).

5. Summary and conclusions

This work examined the directivity properties of nano-antennas made of active CNPs of cylindrical and spherical shapes; the CNPs were excited by a magnetic line source (MLS), in the cylindrical case, and an electric Hertzian dipole (EHD), in the spherical case. The nano-core of the particle consisted of silica, whereas silver was used for the nano-shell material. A canonical, constant frequency, gain model was incorporated inside the dielectric part of the particle. In our studies, particular attention was devoted to the influence of the source location and the optical gain constant on the resulting directivity patterns.

For cylindrical active CNPs, significant variation in the directivity was reported when either the MLS location or the value of the optical gain constant was varied. Specifically, pattern re-shaping from a perfectly monopolar form to a perfectly dipolar pattern (with maximum directivity of 2) was demonstrated for super-resonant CNPs upon the variation of the MLS location - the re-shaping being owed to the coupling strength with the varying MLS location which determines the potency of the underlying resonant dipolar

mode. Moreover, the perfectly symmetric dipolar patterns of the super-resonant CNPs were re-shaped by proper adjustments of the optical gain constant; their main beams pointed in either the $\phi = 0^o$ or $\phi = 180^o$ directions, with the corresponding directivities of almost 3. Moreover, it was found that, once the MLS location for a super-resonant CNP is sufficiently away from its center, the symmetric dipolar mode is excited, and it dominates the behavior of the directivity pattern. The pattern was found to remain unaltered for MLS locations inside the nano-core even at locations further away from the CNP center, as well as for those inside the nano-shell, and outside the CNP at close distances to it. These results are in sharp contrast to those reported for corresponding passive MTM-based configurations at radio frequencies.

The directivity patterns for the active spherical CNPs were shown to be unaffected by variations in the parameters specifying the configurations - even in its super-resonant state for which large amounts of the radiated power are generated by the source. In particular, it was demonstrated that they largely correspond to the pattern of an isolated dipole, i.e., their maximum value remained around 1.5. Unlike the cylindrical case, there is a complete symmetry in the CNP and, consequently, no preferred axis. Thus, as in the passive spherical case treated in [10], the dipolar resonance excited inside the active spherical CNPs does not modify the directivity pattern of the exciting Hertzian dipole. The potential excitation of higher order modes in other configurations of the active CNPs will be considered in a future report.

References

[1] R. E. Collin, *Antennas and Radiowave Propagation*, McGraw-Hill, Int. Ed., 1985.

[2] N. Engheta, and R. W. Ziolkowski, *Metamaterials-Physics and Engineering Applications*, John Wiley & Sons, New York, 2006.

[3] A. Alú, and N. Engheta, "Polarizabilities and effective parameters for collections of spherical nano-particles fromed by pairs of concentric double-negative (DNG), single-negative (SNG) and/or double-positive (DPS) metamaterial layers," *J. Appl. Phys*., Vol. 97, p. 094310, May 2005.

[4] S. Arslanagić, R. W. Ziolkowski, and O. Breinbjerg, "Analytical and numerical investigation of the radiation from concentric metamaterial spheres excited by an electric Hertzian dipole," *Radio Sci*., Vol. 42, 2007, doi:10.1029/2007RS003663.

[5] S. Arslanagić, R. W. Ziolkowski, and O. Breinbjerg, "Analytical and numerical investigation of the radiation and scattering from concentric metamaterial cylinders excited by an electric line source," *Radio Sci*., Vol. 42, 2007, doi:10.1029/2007RS003644.

[6] H. R. Stuart, and A. Pidwerbetsky, "Electrically small antenna elements using negative permittivity radiators," *IEEE Trans. Antennas Propag*., Vol. 54, No.6, pp. 1644-1653, June, 2006.

[7] R. W. Ziolkowski, and A. Erentok "Metamaterial-based efficient electrically small antennas," *IEEE Trans. Antennas Propag.,* Vol. 54, No. 7, pp.2113-2130, July 2006.

[8] A. Erentok, and R.W. Ziolkowski, "Metamaterial-inspired efficient electrically small antennas," *IEEE Ant. Propag.,* Vol. 56, No. 3, 691-707, 2008.

[9] S. J. Oldenburg, G. D. Hale, J. B. Jackson, and N. J. Halas, "Light scattering from dipole and quadrupole nanoshell antennas," *Appl. Phys. Lett*., Vol. 75, No. 8, pp. 1063-1065, Aug. 1999.

[10] A. Alú, and N. Engheta, "Enhanced directivity from sub-wavelength infrared/optical nano-antennas loaded with plasmonic materials or metamaterials," *IEEE Trans. Ant. Propag.*, Vol. 55, No. 11, 3027–3039, 2007.

[11] J. A. Gordon, and R. W. Ziolkowski, "The design and simulated performance of a coated nano-particle laser," *Opt. Express*, Vol. 15, No. 5, 2622-2651, 2007.

[12] S. Arslanagić, and R. W. Ziolkowski, "Active coated nano-particle excited by an arbitrarily located electric Hertzian dipole – resonance and transparency effects," *J. Opt.,* Vol. 12, 024014, 2010.

[13] S. Arslanagić, and R. W. Ziolkowski, "Impact of the excitation source and plasmonic material on cylindrical active coated nano-particles," *Sensors*, Vol. 11, 9109-9120, 2011.

[14] R. W. Ziolkowski, S. Arslanagić, and J. Geng, "Where high-frequency engineering advances opics: active nanoparticles as nanoantennas," to appear in *Optical Nanoantennas*, Eds. A. Alú and M. Agio, Cambridge University Press, London, 2012.